NUCL SCI TECH (2016) 27:19
DOI 10.1007/s41365-016-0020-y

An investigation on the dosimetric impact of hip prosthesis in radiotherapy

Wen-Cheng Shao[1] · Yan-Ling Bai[1] · Wen-Bo Zhao[2] · Pu-Nan Sun[3] · Feng-Li Liu[3]

Received: 7 February 2015 / Revised: 27 April 2015 / Accepted: 3 May 2015 / Published online: 2 March 2016

Abstract The objectives of this study are to evaluate the dosimetric impact of hip prosthesis using ELEKTA linac X-rays and compare the dose perturbations of metallic and nonmetallic hip prostheses. The local dose distributions of typical hip prostheses were calculated for 4, 8, and 15 MV beams by Geant4. Three prosthesis materials were selected in calculation to reveal the relation between material type and local dose perturbations of prostheses. Furthermore, the effect of nominal energy on prosthesis perturbation was also discussed and analyzed. Taking the calculated dose to the hip joint as reference, considerable differences were observed between prostheses and hip joints. In the prosthesis shadow region, the relative dose decreasing was up to 36, 21, and 16 % for the Co–Cr–Mo alloy, titanium alloy, and ceramic prostheses, respectively. In backscattering region, the relative dose increasing was about 1–7 %. Overall, the results show that the dose perturbation effect of prostheses was mainly determined by material type, nominal energy, and density. Among these typical hip prostheses, ceramic prosthesis introduces the lowest dose perturbations.

Keywords Medical linac · Hip prosthesis · Ceramic · Dose perturbation · Monte Carlo method

✉ Yan-Ling Bai
baiyl2126@126.com

[1] Department of Radiation Physics, Harbin Medical University Cancer Hospital, Harbin 150081, China

[2] Beijing Xiao Qing Environmental Engineering Co., Ltd, Harbin office, Harbin 150028, China

[3] School of physical science and technology, Heilongjiang University, Harbin 150001, China

1 Introduction

Total hip replacement (THR) is a widely recommended surgical procedure. There were 76 448 THRs in the UK according to the 2012 National Joint Registry for England and Wales [1]. The number of THRs has risen to about 300,000 every year in the USA [2]. THR is very effective in relieving chronic pain for patients with hip joint necrosis. However, it also can introduce errors in dose calculations [3–5]. Considering the dosimetric importance of prosthesis, the dosimetric impact of hip prosthesis has gradually become a widespread concern in radiotherapy.

An evaluation about the effects of titanium, titanium alloy, and stainless steel prostheses on dose calculation shows that the dose perturbations are determined by the type of material, its density, and its nominal energy [6]. In the other two studies [7, 8], results showed that the dose decreasing was up to 45 % for a metallic hip prosthesis using slice prosthesis configuration, while considerable attenuations (32–55 %) were observed using cubic prosthesis configuration. A series of studies [9–15] approached the accuracy of dose calculation methods for a typical treatment planning system (TPS) in the presence of metallic hip prostheses. The results of these studies showed that most of the typical methods (pencil beam convolution, effective path-length, superposition) more or less overestimate the local dose distributions of prostheses. The algorithm termed Acuros XB performed better than typical methods in commercial TPS; however, it is awaiting full Monte Carlo verifications and not widely applied [10]. Avoidance of directly passing through prostheses was approached, but it has some adverse impacts on treatment plans for photon beams [11]. From the dosimetric perspective, it is still valuable to evaluate the local dose

perturbations by accurate calculation methods, while clinical photon beams pass through hip prostheses.

With the development of ceramic manufacturing technology, ceramic is widely used in manufacturing prosthetic devices [16–18]. However, the dose perturbations of ceramic hip prosthesis are rarely analyzed in most of the previous studies [6–15]. Considering this gap in research on ceramic prosthesis, this study focuses on the differences of relative dose perturbations between titanium alloy, Co–Cr–Mo alloy, and ceramic prostheses, while 4, 8, and 15 MV photon beams pass through these prostheses. Taking the hip joint as a reference, the relative dose perturbations of these hip prostheses were calculated and analyzed by Geant4. These calculation results of various material types are helpful for medical physicists and radiation oncologists and are especially useful to quantify the perturbation differences between ceramic and typical metallic prostheses. More importantly, the results of this study are suitable for the situation of single-photon beams passing through hip prostheses, thus should be corrected by the field weight in a specified treatment plan.

2 Materials and methods

In this section, the elemental composition of a hip prosthesis, the geometry setup of the treatment head, and dose calculation models are provided and illustrated. Two variables (detector angle and detector distance) for prosthesis-detector configuration are introduced for describing the locations of sensitive detectors.

2.1 Relevant parameters used in Monte Carlo simulation

As we know, Monte Carlo particle transport code is widely applied in dose calculation [9–12], and the calculation results of these codes (e.g., MCNP, EGS4, and Geant4) have been accepted as benchmark data for other methods. Consequently, Geant4 Monte Carlo code (version 4.9.2) was selected to calculate the local dose distributions of hip prostheses. The Monte Carlo (MC) simulations of this study were performed on a computing server with two Xeon E5504 processors.

2.2 Elemental composition of typical hip prostheses

Three typical prosthesis materials (titanium alloy, Co–Cr–Mo alloy, and ceramic) were selected in MC simulations. The elemental composition of the hip joint (bone, mass density $= 1.4\,\mathrm{g/cm^3}$) was extracted from the No. 23 report of the ICRP (International Commission on Radiological Protection) [14], while that of hip prostheses were extracted from the reference data supplied by manufacturers. The compositions data listed in Table 1 were used as benchmark data and incorporated into the material functions of the Geant4 detector-construction file.

2.3 Modeling of the linac treatment head

The aim of the modeling is to obtain the photon spectrum of ELEKTA medical linac. For ELEKTA linac, the main components of the treatment head are a target, a primary collimator, two flattening filters, and a secondary collimator system. As shown in Fig. 1, flattening filter No. 1 (difference filter) was located at the basis of the primary collimator only for 15 MV X-ray mode, while flattening filter No. 2 (low-energy X-ray filter) appears at the 4, 8, and 15 MV modes.

2.4 Energy spectra of clinical photon beams

For obtaining photon spectra of ELEKTA linac, the interactions between various electron beams and the target-collimator-filter combined system were simulated. Then, the calculated spectra of the resultant photon beams (Fig. 2) were used as reference data for the 4, 8, and 15 MV virtual sources.

2.5 Modeling of the Monte Carlo calculation

The source-phantom and the prosthesis-detector configurations are illustrated in Fig. 3. As shown in Fig. 3a, virtual photon sources (4, 8, and 15 MV) were placed above a cubic water phantom, and the spheroid hip prosthesis with a 4 cm diameter is located at the phantom center. Figure 3b (generated by OPENGL) depicts the interaction between the primary ray and the hip prosthesis. It also shows a sketch of the prosthesis-detector configuration. Several sensitive detectors were placed at an interval of 5° surrounding the prosthesis. As illustrated in Fig. 3c, the geometric parameter θ is termed as detector angle, and it is defined as the angle between the beam axis and the vector connecting the prosthesis and the detector center. The parameter d (detector distance) quantify the distance between the prosthesis surface and detector centers. In this study, several simulations were accomplished using various d (5, 10, 15, and 20 mm) to reveal the relation between prosthesis dose perturbations and detector distance.

2.6 The dose differences between hip prostheses and hip joint

In this study, the dose differences between prostheses and the hip joint are quantified by a variable RDP (relative dose perturbation), which can be expressed as follows:

Table 1 (a) Elemental composition of typical hip prostheses. (b) Physical properties of typical hip prostheses

Element	Fraction by weight				Element	Fraction by weight			
	Hip joint (%)	Titanium alloy	Co–Cr–Mo alloy	Ceramic		Hip joint	Titanium alloy	Co–Cr–Mo alloy	Ceramic
(a)									
H	7.337	0.015 %	–	–	Rb	0.002 %	–	–	–
C	25.475	0.1 %	0.1 %	–	Sr	0.003 %	–	–	–
N	3.057	0.05 %	0.25 %	–	Pb	0.001 %	–	–	–
O	47.893	0.2 %	–	–	Ti	–	88.04 %	–	–
F	0.025	–	–	–	Al	–	6.8 %	–	–
Na	0.326	–	–	–	V	–	4.5 %	–	–
Mg	0.112	–	–	–	Co	–	–	61.9 %	–
Si	0.002	–	1 %	–	Cr	–	–	28 %	–
P	5.095	–	–	–	Mo	–	–	6 %	–
S	0.173	–	–	–	Mn	–	–	1 %	–
Cl	0.143	–	–	–	Ni	–	–	1 %	–
K	0.153	–	–	–	Al_2O_3	–	–	–	82 %
Ca	10.190	–	–	–	ZrO_2	–	–	–	17 %
Fe	0.008	0.3 %	0.75 %	–	SrO	–	–	–	1 %
Zn	0.005	–	–	–					

	Titanium alloy	Co–Cr–Mo alloy	Ceramic
(b)			
Mass density	4.5 g/cm^3	8.0 g/cm^3	3.98 g/cm^3
Relative electron density	3.4	6.6	3.5

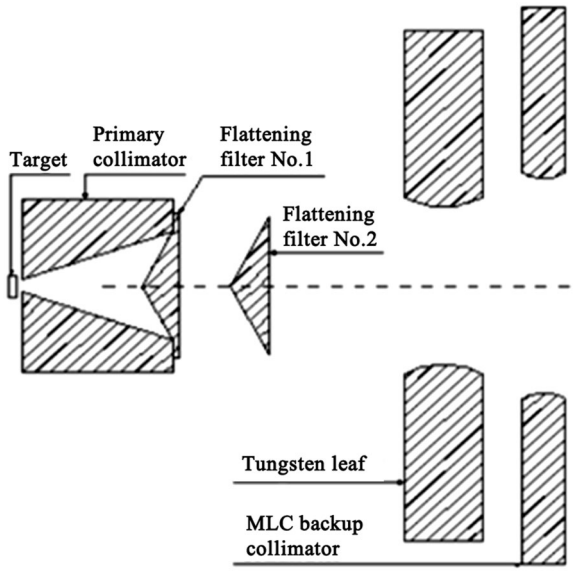

Fig. 1 Geometry setup of the treatment head

$$RDP(\theta, d) = D(\theta, d)_{m_i} - D(\theta, d)_{\text{bone}}, \quad (1)$$

where m_i is the abbreviation of prosthesis material, θ is the detector angle, d is the detector distance, $D(\theta, d)_{m_i}$ is the calculated dose for mi, and $D(\theta, d)_{\text{bone}}$ is the calculated dose for the hip joint.

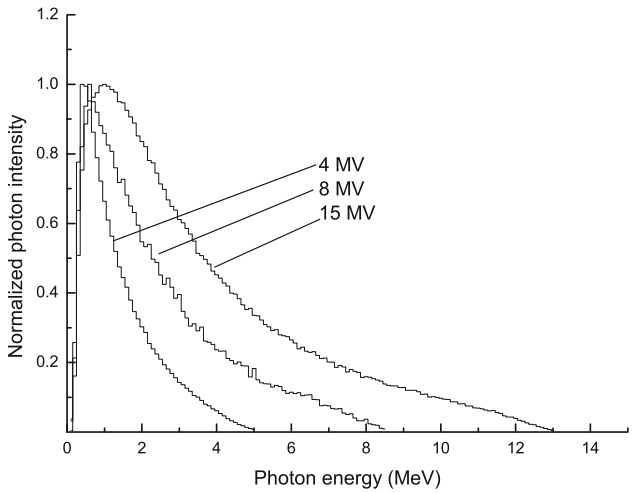

Fig. 2 Calculated photon spectra for 4, 8, and 15 MV clinical beams

3 Results and discussion

3.1 Local dose distributions of typical hip prostheses

In this section, the calculated dose distributions of typical prostheses are illustrated in Fig. 4. In most cases, about 2 billion events were simulated in each Geant4 Run-

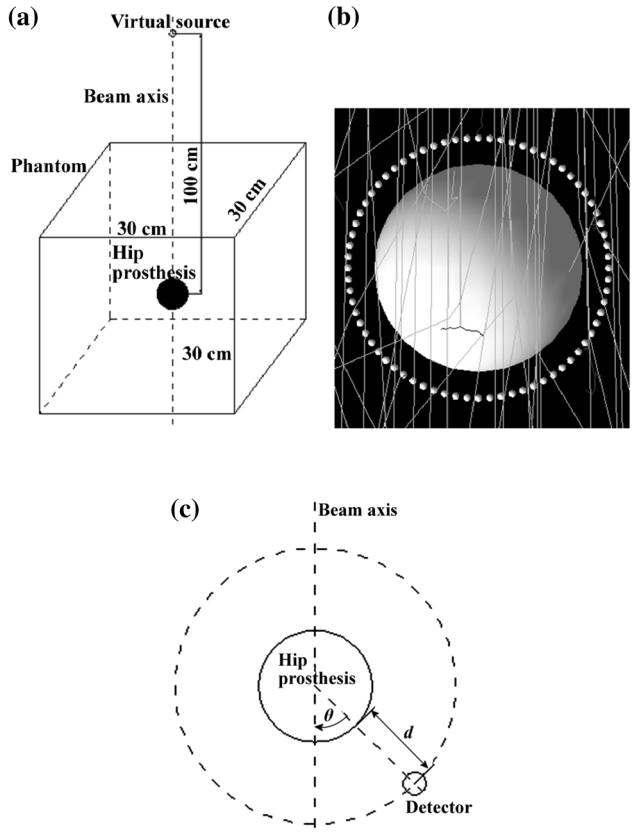

Fig. 3 The MC calculation model: **a** source-phantom system; **b** prosthesis-detector system; **c** illustration of two geometry setup parameters for prosthesis-detector system

Action, while the relative errors are smaller than 0.05. To simplify notations, the titanium alloy prosthesis, Co–Cr–Mo alloy prosthesis, and ceramic prostheses were, respectively, abbreviated as TC4, CCM, and ceramic.

As shown in Fig. 4, the calculated dose for the hip joint increases approximately linearly with θ (detector angle). For hip prostheses, an inflection point appears at each dose-angle curve. The inflection point becomes the critical point that divides the entire angle range into two regions with different dose-angle variation laws. Compared to the hip joint, the dose distributions of prostheses show several obvious characteristics. Firstly, the inflection angles (correspondent θ of inflection points) of these prostheses are approximately the same for a specified d (detector distance), and it decreases with d. Secondly, the calculated dose increases with θ in accordance with a power function, while θ is smaller than the inflection angles (shadow region). Thirdly, the calculated dose for the prostheses is approximately the same as that for the hip joint for 10, 15, and 20 mm detector distances, while θ is larger than the inflection angles (scattering region).

Overall, the calculated dose is smallest for CCM and largest for ceramic in the prosthesis shadow region. In the prosthesis scattering region, the largest calculated dose for the prostheses appears for a 15 MV beam, while the smallest dose was observed for a 4 MV beam. In this region, it increases about 1–7 % for 8 and 15 MV beams at a 5 mm detector distance.

3.2 Local dose differences between hip prostheses and hip joint

In this section, the relative dose perturbation (RDP) is calculated and illustrated in Fig. 5.

As shown in Fig. 5, each RDP-angle curve has an inflection point. The inflection angles are approximately $60°, 50°, 45°$, and $40°$ for 5, 10, 15, and 20 mm, respectively. The expression of RDP implies that the positive RDPs quantify the relative dose increases of the prostheses compared to the hip joint, while the negative RDPs quantify the relative dose decreases. In the prosthesis shadow region, CCM and ceramic show the smallest and largest RDPs, respectively. For a specified hip prosthesis, RDP is minimized at the minimum θ, and then increases with the θ according to the power function law. Finally, it nearly approaches zero at the inflection point. In the prosthesis scattering region, the RDPs are very sensitive to the nominal energy and are nearly zero for the 4, 8, and 15 MV beams, while the detector distances are 10, 15, or 20 mm. However, the RDPs are slightly positive (1–7 %) for the 8 and 15 MV beams at a 5 mm detector distance, which indicates the calculated dose for the prostheses is slightly larger than that of the hip joint.

Generally, the differences between this study and previous reports [6–8] mainly originate from the differences in geometric setup parameters, radiation source characteristics, and calculation codes. Firstly, a spheroid configuration was used in our Monte Carlo modeling, but cubic or thin slice configuration was used in most previous works. Besides, the deviations of geometric setup parameters (e.g., source-surface distance, source-axis distance) can also introduce differences of calculated dose perturbations. Secondly, the differences of linac X-ray characteristic (e.g., photon spectrum and photon intensity) probably influence the calculation results. Thirdly, the Geant4 Monte Carlo toolkit (standard EM physics process) was applied in evaluating the RDP of hip prosthesis in this study, but the EGS4 or EGSnrc systems were mainly utilized in earlier works. Taking together, the combination of above factors has important dosimetric implications when calculation results of different investigations were compared.

3.3 Impact of nominal energy on relative dose perturbations

In the prosthesis shadow region, the RDP values for the Co–Cr–Mo alloy, titanium alloy, and ceramic hip

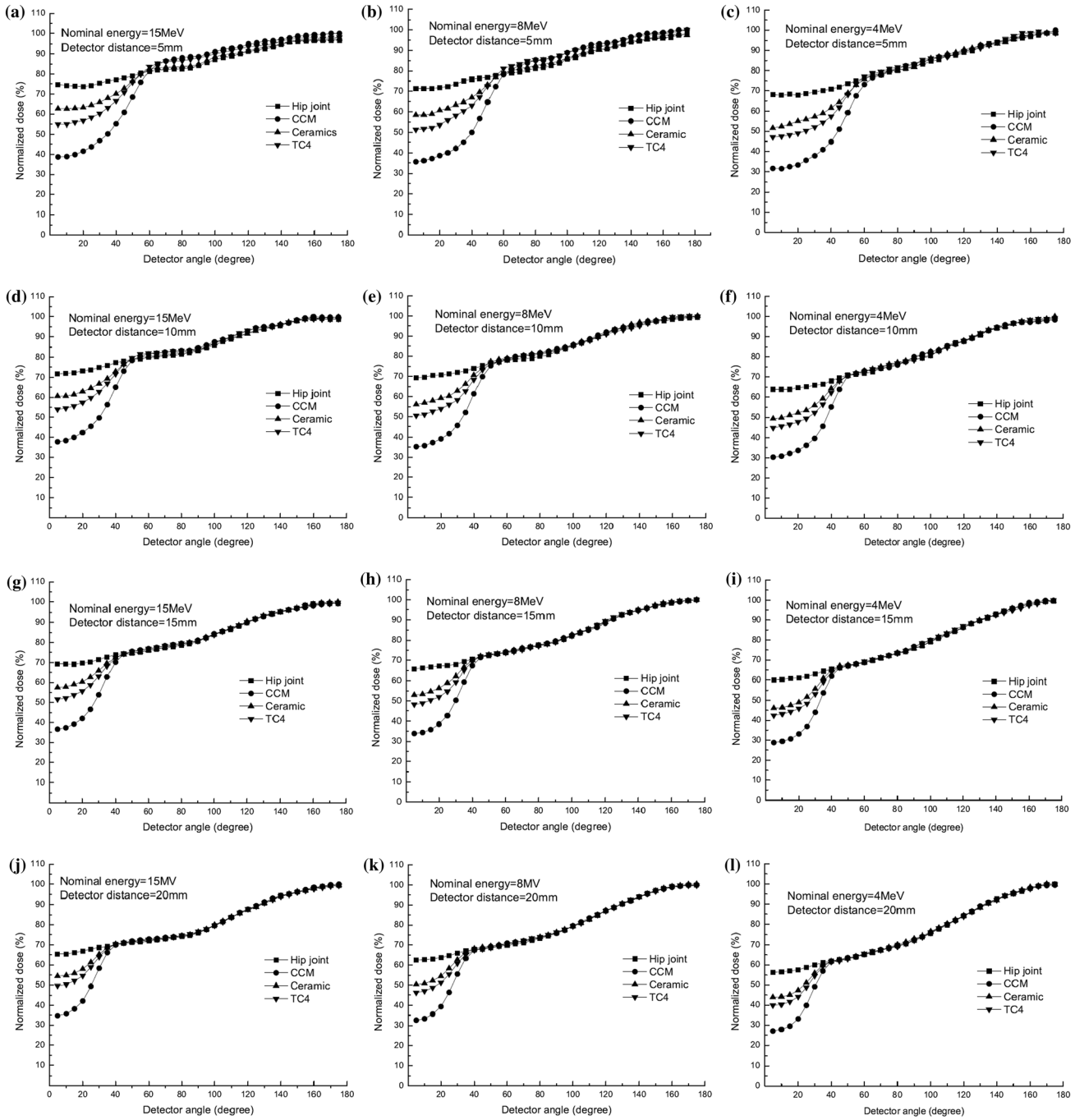

Fig. 4 Local dose distributions for 4, 8, and 15 MV photon beams

prostheses are almost 37, 22, and 16 % for the 4 MV beam; 35, 21, and 14 % for the 8 MV beam; 35, 21, and 13 % for the 15 MV beam. Obviously, the differences of maximum RDP values between 4, 8, and 15 MV beams are smaller than 2 % for specified material type and detector distance. In other words, nominal energy is not the dominant factor influencing prosthesis perturbations in this region. That is because the beam with higher nominal energy also shows stronger penetrating power toward the water above the prostheses, when prostheses show stronger absorption and scattering compared to the hip joint. For this region, material type greatly influences RDPs, which is due to substantial attenuations by these prostheses. Thus, the prostheses with a higher atomic number or density are more likely to introduce stronger perturbations, owing to its stronger absorption or scattering.

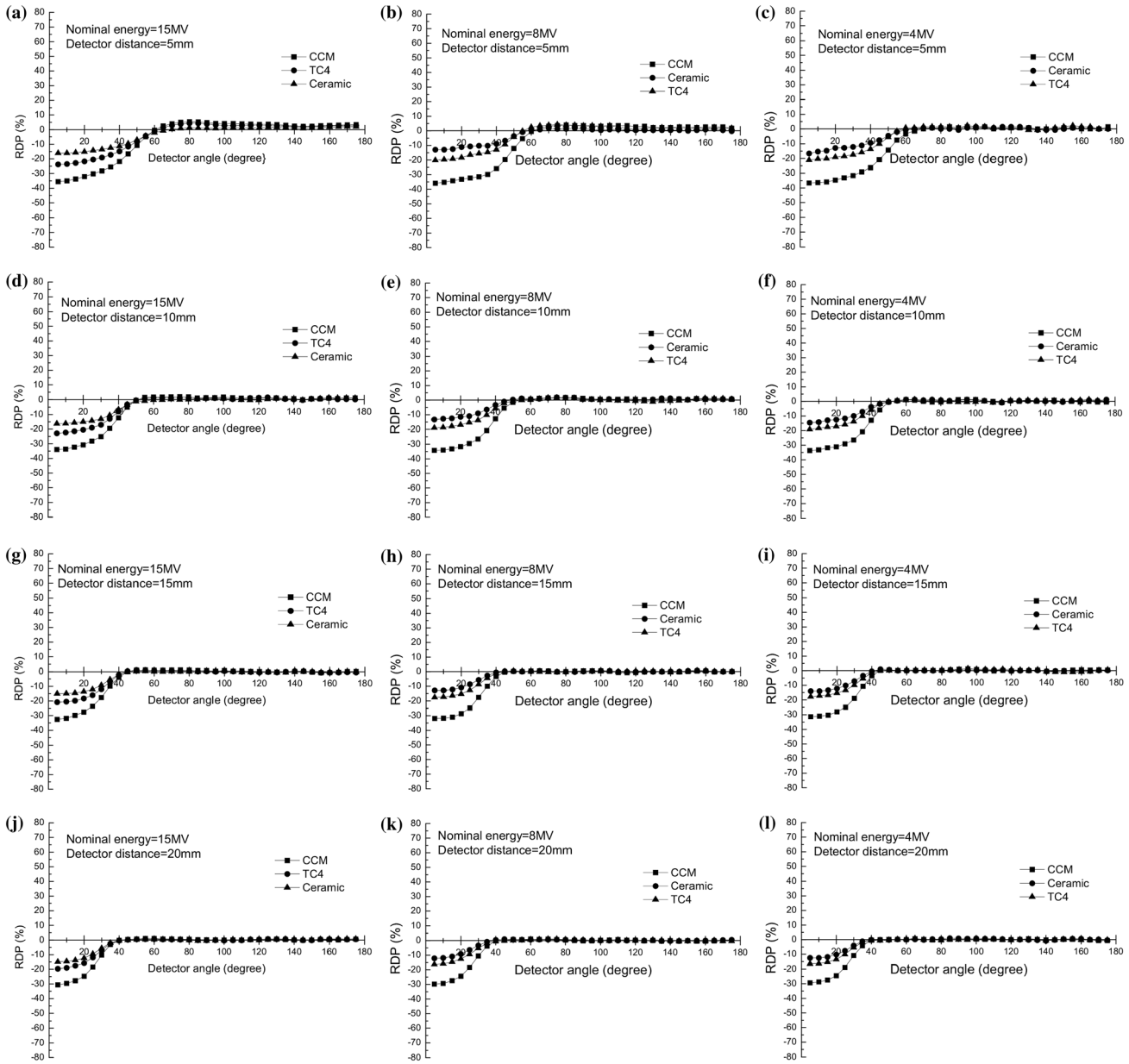

Fig. 5 Calculated RDP values for 4, 8, and 15 MV photon beams

In the prosthesis scattering region, however, the RDPs are greatly influenced by nominal energy or detector distance. Except for the 5 mm detector distance, almost no dose perturbations were observed for 4, 8, and 15 MV beams. The primary ray was not attenuated by the prostheses before reaching these detectors belonging to this region; therefore, the water-generated electrons and prosthesis-generated Compton electrons mainly influence prosthesis dose perturbations. The water-generated electrons remain approximately constant after the replacement of the hip joint by prosthesis. Thus, the RDPs mainly depend on the Compton electrons generated by the prostheses. In other words, the calculated dose will increase with the yield of prosthesis-generated electrons, while detector distance is shorter than the range of these electrons. On the contrary, an increased electron yield hardly introduces any dose perturbations, while detector distances are larger than the Compton electron range. In most cases, photon beams with higher nominal energy are inclined to generate Compton electrons with a relatively higher kinetic energy. Thus, the dose perturbations for a 15 MV beam are stronger than that of 4 and 8 MV beams in this region, and it reaches up to 7 % for a 5 mm detector distance.

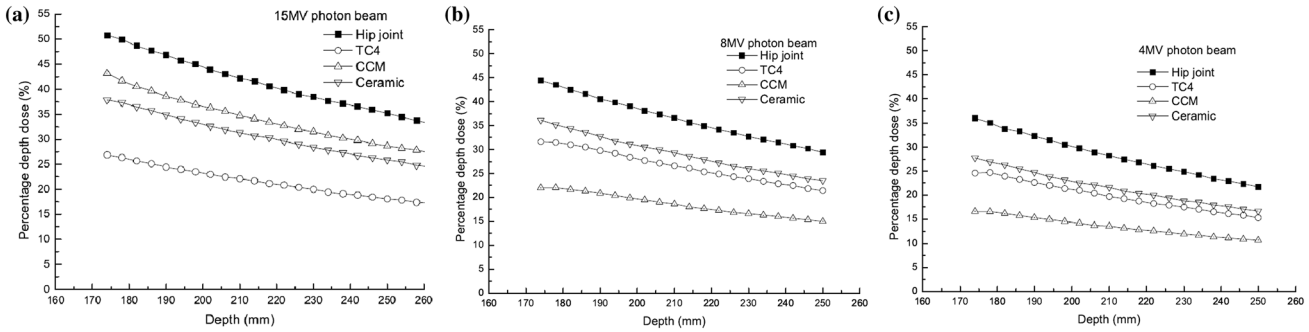

Fig. 6 Percentage depth dose beneath prostheses (normalized by the maximum dose of hip joint)

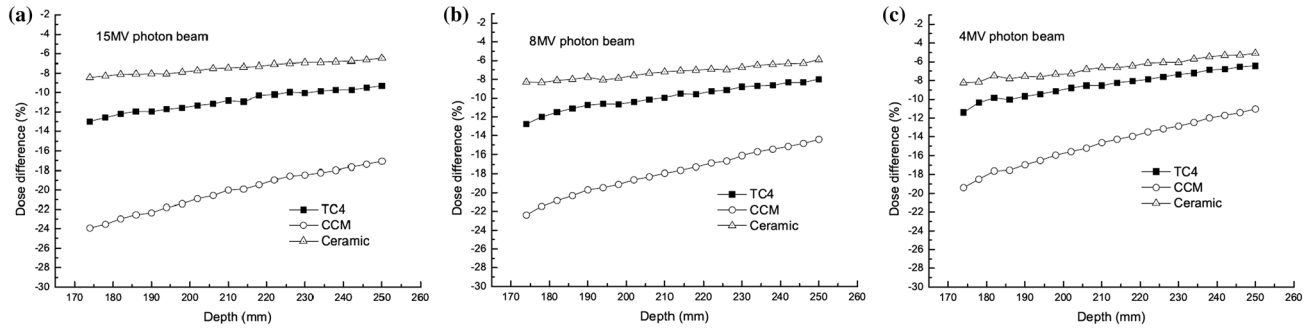

Fig. 7 Depth dose differences between prostheses and hip joint

3.4 Depth dose distribution beneath prostheses

In this section, percentage depth dose (Fig. 6) beneath the prosthesis was calculated for 4, 8, and 15 MV beams. The depth dose differences (Fig. 7) between the prostheses and hip joint were introduced to reveal the relation between material type and prosthesis attenuations.

Obviously, 4, 8, and 15 MV beams were intensively attenuated by these prostheses, while the dose decrease closely depends on the atomic number or density of the prostheses. In detail, CCM illustrated the largest dose decrease; on the contrary ceramic shows the smallest decrease, owing to its smaller atomic number or density. To quantify the decrease of the depth dose, the authors calculated the dose differences between the prostheses and hip joint and plotted these calculated differences in Fig. 7. As shown in Fig. 7, depth dose differences increase with depth and were determined by the atomic number or density. So far, we have evaluated the dosimetric perturbations of three typical prostheses and offered useful data for medical physicists and radiation oncologists.

4 Conclusion

In this investigation, several simulations were performed to evaluate the relative dose perturbations (RDPs) of various hip prostheses for 4, 8, and 15 MV clinical beams by Geant4. In the prosthesis shadow region, the maximum dose perturbations are 37, 21, and 16 % for the Co–Cr–Mo alloy, titanium alloy, and ceramic hip prostheses, respectively. In the prosthesis scattering region, the maximum perturbations are 1, 4, and 7 % for 4, 8, and 15 MV clinical beams at a 5 mm detector distance.

Among these patients with a hip prosthesis, the metallosis probability of ceramic prostheses is much smaller than that of metallic hip prostheses [16]. From the dosimetric prospective, a ceramic prosthesis introduces the lowest dose perturbations between typical prosthesis materials, while photon beams pass through. The maximum relative perturbations of a ceramic prosthesis are smaller than 2 % in the scattering region; the relative perturbations caused by prosthesis attenuations are smaller than 16 % in the shadow region. Taken together, ceramic is more recommended in prosthetic device manufacture.

Considering the strong dose perturbations of metallic hip prostheses, medical physicists should select proper gantry angles to prevent clinical beams from passing through it. If that is unavoidable, a possible solution is to let clinical beams pass through the PTV (planning target volume) before passing through metallic prostheses. This is useful for partly lowering the dose perturbations, because the perturbations of the scatting region are much smaller than that of shadow region. For the fields passing through the prostheses, another effective method to lower the dose perturbations in a specified treatment plan is to minimize its field weight.

Acknowledgments This study was supported by Heilongjiang Province Natural Science Foundation (No. A200805), the Education Department of Heilongjiang Province (No. 12521425), and the post-doctoral research start-up funds of Heilongjiang Province (No. LBH-Q11013).

References

1. V. Wylde, E. Marques, N. Artz et al., Effectiveness and cost-effectiveness of a group-based pain self-management intervention for patients undergoing total hip replacement: feasibility study for a randomized controlled trial. Trials **15**, 176 (2014). doi:10.1186/1745-6215-15-176
2. J.N. Katz, E.A. Wright, J.J.Z. Polaris et al. Prevalence and risk factors for periprosthetic fracture in older recipients of total hip replacement: a cohort study. BMC Musculoskelet. Disord. **15**, 168. doi:10.1186/1471-2474-15-168
3. M. Bazalova, L. Beaulieu, S. Palefsky et al., Correction of CT artifacts and its influence on Monte Carlo dose calculations. Med. Phys. **34**, 2119–2132 (2007). doi:10.1118/1.2736777
4. L. Yu, H. Li, J. Mueller et al., Metal artifact reduction from reformatted projections for hip prostheses in multislice helical computed tomography: techniques and initial clinical results. Invest. Radiol. **44**, 691–696 (2009). doi:10.1097/RLI.0b013e3181b0a2f9
5. X.Y. Gong, E. Meyer, X.J. Yu et al., Clinical evaluation of the normalized metal artefact reduction algorithm caused by dental fillings in CT. Dentomaxillofac Radiol. **42**, 20120105 (2013). doi:10.1259/dmfr.20120105
6. S. Çatl, G. Tanır, Experimental and Monte Carlo evaluation of Eclipse treatment planning system for effects on dose distribution of the hip prostheses. Med. Dosim. **38**, 332–336 (2013). doi:10.1016/j.meddos.2013.03.005
7. G.X. Ding, C.W. Yu, A study on beams passing through hip prosthesis for pelvic radiation treatment. Int. J. Radiat. Oncol. Biol. Phys. **51**, 1167–1175 (2001). doi:10.1016/S0360-3016(01)02592-5
8. A. Mesbahi, F.S. Nejad, Dose attenuation effect of hip prostheses in a 9-MV photon beam: commercial treatment planning system versus Monte Carlo calculations. Radiat. Med. **25**, 529–535 (2007). doi:10.1007/s11604-007-0181-z
9. C. Reft, R. Alecu, I.J. Das et al., Dosimetric considerations for patients with HIP prostheses undergoing pelvic irradiation. Report of the AAPM Radiation Therapy Committee Task Group 63. Med. Phys. **30**, 1162–1182 (2003). doi:10.1118/1.1565113
10. J. Ojala, The accuracy of the Acuros XB algorithm in external beam radiotherapy-a comprehensive review. Int. J. Cancer Thera. Oncol. **2**, 020417 (2014). doi:10.14319/ijcto.0204.17
11. S. Rana, C. Cheng, Y. Zheng et al., Dosimetric study of uniform scanning proton therapy planning for prostate cancer patients with a metal hip prosthesis, and comparison with volumetric-modulated arc therapy. J. Appl. Clin. Med. Phys. **15**, 335–348 (2014). doi:10.1120/jacmp.v15i3.4611
12. I. Das, S. Chang, C. Cheng et al., Dosimetric comparison of high-Z inhomogeneity in IMRT: a collaborative study. Med. Phys. **34**, 2592 (2007). doi:10.1118/1.2761525
13. P.J. Keall, J.V. Siebers, R. Jeraj et al., Radiotherapy dose calculations in the presence of hp prostheses. Med. Dosim. **28**, 107–112 (2003). doi:10.1016/S0958-3947(02)00245-5
14. A.B. Hwang, E. Kinsey, P. Xia, Investigation of the dosimetric accuracy of the isocenter shifting method in prostate cancer patients with and without hip prostheses. Med. Phys. **36**, 5221–5227 (2009). doi:10.1118/1.3245882
15. R. Roberts, How accurate is a CT-based dose calculation on a pencil beam TPS for a patient with a metallic prosthesis? Phys. Med. Biol. **46**, N227–N234 (2001). doi:10.1088/0031-9155/46/9/402
16. C.A. Oliveiraa, I.S. Candelériaa, P.B. Oliveiraa et al., Metallosis: a diagnosis not only in patients with metal-on-metal prostheses. Eur. J. Radiol. Open **2**, 3–6 (2015). doi:10.1016/j.ejro.2014.11.001
17. T. Roy, D. Choudhury, S. Ghosh et al., Improved friction and wear performance of micro dimpled ceramic-on-ceramic interface for hip joint arthroplasty. Ceram. Int. **41**, 681–690 (2015). doi:10.1016/j.ceramint.2014.08.123
18. E. Sariali, S. Klouche, P. Mamoudy, Ceramic-on-ceramic total hip arthroplasty: is squeaking related to an inaccurate three-dimensional hip anatomy reconstruction? Orthop. Traumat. Surg. Res. **100**, 437–440 (2014). doi:10.1016/j.otsr.2014.01.009
19. K. Jabbari, H.S. Anvar, M.B. Tavakoli et al., Monte Carlo simulation of siemens ONCOR linear accelerator with BEAMnrc and DOSXYZnrc code. J. Med. Signals Sens. **3**, 172–179 (2013)
20. R.S. Vishwakarma, T.P. Selvam, S. Sahoo et al., Monte Carlo-based investigation of water-equivalence of solid phantoms at ^{137}Cs energy. J. Med. Phys. **38**, 158–164 (2013). doi:10.4103/0971-6203.121192
21. X. Dong, W. Luo, K. Yue et al., Monte carlo study on 6 MV photon beams of a CyberKnifestereotactic radiosurgery system. Nucl. Sci. Tech. **1**, 16–19 (2010). doi:10.13538/j.1001-8042/nst.21.16-19
22. J. Zhu, W. Ma, Y. Zhu et al., Monte-Carlo simulation of pinhole collimator of a small field of view gamma camera for small animal imaging. Nucl. Sci. Tech. **1**, 37–41 (2009). doi:10.13538/j.1001-8042/nst.20.37-41
23. M. Asai, J. Apostolakis, G. Cosmo et al. Introduction to Geant4. http://geant4.web.cern.ch/geant4/UserDocumentation/Welcome/IntroductionToGeant4/html/index.html
24. International Commission on Radiological Protection. *Report of the Task Group on Reference Man*. ICRP Publication 23. (Pergamon Press, Oxford, 1975)